Endothelin Receptor in Virus-Like Particles: Ligand Binding Observed by Fluorescence Fluctuation Spectroscopy†

Lenka Zemanová,‡ Andreas Schenk,‡ Nicholas Hunt,§ G. Ulrich Nienhaus,‡,|| and Ralf Heilker*,⊥

Department of Biophysics, University of Ulm, Albert Einstein Allee 11, D-89081 Ulm, Evotec OAI, Schnackenburgallee 114, D-22525 Hamburg, Germany, Department of Physics, University of Illinois at Urbana-Champaign, 1110 West Green Street, Urbana, Illinois 61801, and Department of Integrated Lead Discovery, Boehringer Ingelheim Pharma GmbH & Co. KG, Birkendorfer Str.65, D-88397 Biberach, Germany

Received October 24, 2003; Revised Manuscript Received May 18, 2004

ABSTRACT: The functional analysis of transmembrane receptor proteins is frequently hampered by the difficulty to produce sufficiently homogeneous receptor preparations that preserve the physiological biomembrane integration of the receptor protein. To improve the receptor protein density in the lipid bilayer and to maintain the physiological lipid−protein environment, a novel method has been established that enables the selective integration of transmembrane receptors into a virus-like particle (VLiP). Here we have studied the binding of tetramethylrhodamine-labeled endothelin-1 (TMR-ET-1) to VLiP-integrated endothelin A receptor (ET_AR) by fluorescence fluctuation spectroscopy. The concentration of TMR-ET-1 was determined by fluorescence correlation spectroscopy (FCS). These measurements also confirmed that the free ligand is monomeric in solution in our experiments. Fluorescence intensity distribution analysis (FIDA) was used to quantify the fraction of ligands bound to ET_ARs in the VLiPs. For the interaction between ET-1 and VLiP-integrated ET_ARs, K_D values of 0.5 nM and 0.3 nM were determined from ligand and receptor titration experiments, respectively. For comparison, a FIDA analysis was also carried out with ET_ARs in membrane fragments derived from an ET_AR-overexpressing mammalian cell line, which yielded a similar K_D of 0.2 nM. In addition, we examined the binding competition of a set of reference compounds to VLiP-ET_ARs in the presence of ET-1 and obtained K_i values similar to those reported in the literature. Our results demonstrate that integration into VLiPs does not change the binding properties of the ET_ARs. FIDA analysis of VLiP-integrated receptors shows great promise for highly miniaturized and fast compound testing in the pharmaceutical industry.

Approximately 45% of all known pharmaceutical drugs are directed against transmembrane receptors (*1*), largely G-protein coupled receptors (GPCRs).[1] Economically, these 7-transmembrane receptors are thus the most important class of therapeutic targets (*2*), and it is of particular interest to find novel agonists and antagonists for the vast number of GPCRs, in combination with a preferably homogeneous optical assay.

Binding studies with transmembrane receptors can be performed in a number of systems and environments. Ligand interactions can be investigated directly on the cell surface or in membrane fragments from cells overexpressing the receptor of interest. However, the analysis may be compromised by high background levels of other membrane proteins that are expressed endogenously by the transfected host cell. Alternatively, the respective receptor may be purified from overexpressing cells or tissue. This biochemical purification, however, typically requires the exchange of the physiological lipid/lipid−protein environment by a detergent micelle, which may modify the binding properties of the receptor. In an ideal receptor preparation format, a high enrichment of the receptor of interest would be combined with the receptor's integration into its natural lipid/lipid−protein environment.

With this aim in mind, a novel insect-cell-based co-expression system was designed at Evotec OAI, which is based on the use of a retroviral budding protein named Gag. Retroviruses possess a protein capsid enclosed by a lipid bilayer that is derived from the host cell plasma membrane in the budding process (*3*−*8*). Studies with several retroviruses have demonstrated that the Gag poly-protein expressed in the absence of other viral components is self-sufficient for particle formation and budding at the cell surface. Formation of retrovirus-like particles upon expression of the Gag precursor in insect cells has been demonstrated by several groups (*3*−*10*). These Gag particles resemble immature lentivirus particles and are efficiently

† This work was supported by the University of Ulm, Deutsche Forschungsgemeinschaft (GRK 328 and SFB569), and Boehringer Ingelheim Pharma GmbH & Co. KG.

* To whom correspondence should be addressed. Ralf.Heilker@bc.boehringer-ingelheim.com.

‡ University of Ulm.

§ Evotec OAI.

|| University of Illinois at Urbana-Champaign.

⊥ Boehringer Ingelheim Pharma GmbH & Co.

[1] Abbreviations Used: VLiP, virus-like particle; TMR, tetramethylrhodamine; ET-1, endothelin 1; ET_AR, endothelin A receptor; GPCR, G-protein coupled receptor; BSA, bovine serum albumin; CHO cells, Chinese hamster ovary cells; BHK cells, baby hamster kidney cells; FCS, fluorescence correlation spectroscopy; FIDA, fluorescence intensity distribution analysis; ACF, autocorrelation function; PCH, photon counting histogram; HTS, high-throughput screening.

10.1021/bi035901+ CCC: $27.50
Published on Web 06/19/2004

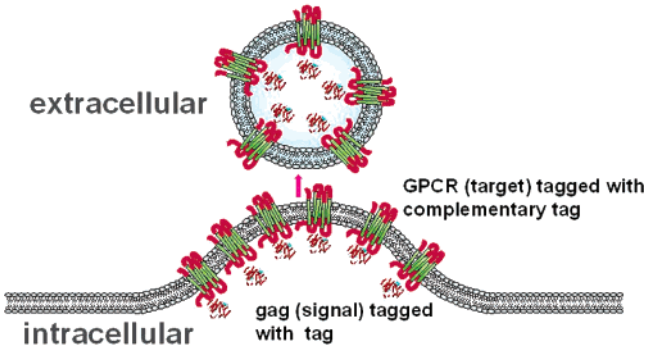

FIGURE 1: Schematic representation of a VLiP budding from a host cell incorporating a GPCR of interest. A Gag-tag fusion protein (violet) is coexpressed in a cellular system with the GPCR (red: extracellular domains, green: transmembrane domains), which carries the complementary peptide tag at the C-terminus. Expression of a retroviral Gag protein in the host cells results in the accumulation of the Gag protein at the plasma membrane due to signals present within the N-terminal portion of the Gag protein. High concentrations of this protein at the plasma membrane induce a budding process, by which the VLiPs are released into the extracellular medium where they can be harvested. The incorporation of the respective target GPCR within the envelope of the VLiPs is the result of a strong specific interaction of the peptide tag covalently attached to the C-terminus of the Gag protein with the complementary, specific peptide tag attached to the C-terminus of the GPCR.

assembled and released by budding from the insect cell plasma membrane.

Evotec OAI has established a method that selectively incorporates transmembrane proteins (e.g., GPCRs) into virus-like particles (VLiPs). For this purpose, the transmembrane protein of interest (the "target molecule") is coexpressed in insect cells together with the Gag protein from Moloney murine leukemia virus, which leads to viral particle formation and budding at the cell surface. The target molecule at its cytoplasmic portion and the Gag protein at its C-terminus contain amino acid sequences that enable their interaction (Hunt et al., manuscript in preparation). By virtue of this interaction, the Gag protein recruits the target molecule into the budding VLiP. The resulting chimeric VLiPs are released into the extracellular medium (Figure 1). By these means, the endothelin A receptor (ET_AR), a GPCR that mainly elicits the vasoconstrictive effects of the endothelin 1 (ET-1) peptide hormone (*11*, *12*), was integrated into VLiPs (*13*). The chimeric VLiPs constitute a concentrated source of the ET_AR and thereby show great potential for fluorescence fluctuation spectroscopy techniques, which require very high purity of the samples. Despite the promising features of the VLiPs, the important question remains whether integration of the ET_AR into the VLiP affects the binding properties of the receptor. To address this question, we performed binding studies with TMR-ET-1. Furthermore, we compared the VLiP-ET_AR with receptors integrated in membrane fragments of mammalian cells, and we also examined some known ligand competitor compounds.

For the study of the interaction between TMR-ET-1 and VLiP-integrated ET_AR, we employed fluorescence fluctuation spectroscopy using a confocal microscope. Using FCS (*14*−*16*), we determined the diffusion coefficient and the concentration of TMR-ET-1 in solution. The statistical analysis of the brightness of the fluorescence fluctuations yielded information about the number of fluorophores attached to the diffusing entity. This allowed us to study association reactions of VLiPs and membrane fragments, which carry a large number of receptors, and thus, many binding sites for fluorescently labeled ligands. The distribution of the numbers of photons per time bin can be analyzed by using two slightly different statistical methods, photon counting histogram (PCH) analysis, which has been developed by Chen and co-workers (*17*), and FIDA, introduced by Kask and co-workers (*18*). The FIDA technique has already been applied to membrane receptor assays using membrane fragments derived from mammalian cells overexpressing the receptor (*19*−*21*). In this work, we have used the FIDA technique to determine equilibrium binding constants of tetramethylrhodamine (TMR) labeled ET-1 to VLiP-integrated ET_AR and ET_AR in membrane fragments. We have also measured the inhibition constants of three ET-1 competitors.

Our results indicate that the ET_ARs integrated into VLiPs exhibit essentially identical binding properties as ET_ARs that are integrated into membrane fragments derived from mammalian cells. VLiP-integrated GPCRs are particularly well suited for FIDA applications in drug screening (e.g., search for competitive agonists and antagonists), using a highly miniaturized format with low concentrations of bioreagents. Such an assay regimen is of utmost interest and importance for the pharmaceutical industry, which is constantly searching for assay approaches applicable to the vast number of receptors being discovered by numerous functional genomics programs.

EXPERIMENTAL PROCEDURES

Microscope. A 514-nm light from an argon/krypton ion laser (model 164, Spectra-Physics, Mountain View, CA) was focused on the sample by using a dichroic mirror (Q525LP, AHF, Tübingen, Germany) and a water immersion objective (UPAPLO 60×/1.2W, Olympus, Hamburg, Germany) in an inverted microscope (Axiovert 35, Carl Zeiss, Göttingen, Germany). The emitted photons were collected through the same objective, focused on a confocal pinhole (50-μm diameter), and detected by an avalanche photodiode (SPCM-AQR-14, Perkin-Elmer, Vaudreuil, Canada). The observed spectral band was limited to wavelengths between 557 and 607 nm using a band-pass filter (HQ 582/50, AHF) and a long pass filter (HQ 700/300, AHF). Movement of the confocal volume through the sample was achieved by scanning the sample in a circle of 30-μm radius with a velocity of 0.8 μm/ms using a piezoelectric scanning stage (Tritor 102 Cap, Piezosysteme Jena, Jena, Germany).

The photodiode output signals were autocorrelated in a digital correlator (ALV-5000/E, ALV, Langen, Germany), acquired by using a computer card for single-photon counting (TimeHarp100, Pico-Quant, Berlin) or simply collected as a function of time using a homemade computer card. The latter card enables data analysis with our own data acquisition software.

Materials. Cloned human ET_AR in VLiPs was produced at Evotec OAI, Hamburg (Nicholas Hunt, manuscript in preparation). The supernatant of the *Spodoptera frugiperda* (Sf9) cell culture was concentrated and stored in 50 mM Tris/HCl pH 7.4, 1 mM $CaCl_2$, 0.2% bovine serum albumin (BSA), and 0.1% NaN_3 at −80 °C. Before use, it was thawed on ice and homogenized by ultrasonication in sonication bath

for 1 min, as recommended by the manufacturer, and diluted with 50 mM Tris/HCl pH 7.4, 1 mM $CaCl_2$, 0.2% BSA. After centrifugation at 3000*g* for 1 min, the supernatant was used for the binding assay. Cloned human ET_AR produced in Chinese hamster ovary (CHO) cells was provided as membrane fragments by BioSignal Packard, Montréal, Canada. The membrane fragments were stored at −80 °C in 50 mM Tris/HCl pH 7.4, 10% glycerol, 1% BSA. For the binding assay, they were thawed on ice and diluted in 50 mM Tris/HCl pH 7.4, 1 mM $CaCl_2$, 0.2% BSA.

The peptide substrate ET-1, consisting of 21 amino acids, was labeled with 5-carboxy TMR on the side chain of the lysine. The synthesis of the peptide and its labeling with TMR were carried out by Evotec OAI, Hamburg, Germany, using solution phase chemistry. The labeled peptide was finally characterized by liquid chromatography/mass spectrometry (LC/MS) and matrix assisted laser desorption ionization time-of-flight (MALDI-TOF) analysis. The label position was confirmed by mass spectrometry after enzymatic digestion of TMR-ET-1 (Lopez-Calle, E.; Evotec OAI; personal communication). We have additionally confirmed the correct size of the single-TMR-labeled peptide by MALDI-TOF as 2902 Da. Using a CHO cell line overexpressing the ET_AR we could demonstrate binding to the cell surface and internalization of TMR-ET-1 at a low nanomolar concentration, which could be competed by an ET_AR antagonist (data not shown). Unlabeled ET-1 was purchased from Bachem Feinchemikalien, Bubendorf, Switzerland, and competitors BQ-123, sulfisoxazole, and sarafotoxin 6b from Tocris Cookson, Avonmouth Bristol, UK. All ligands and competitors, ET-1, TMR-ET-1, BQ-123, sulfisoxazole and sarafotoxin 6b were received in lyophilized form, then dissolved in dimethyl sulfoxide, aliquoted, and stored at −80 °C. For the binding or competition assay, they were diluted in 50 mM Tris/HCl pH 7.4, 1 mM $CaCl_2$, 0.2% Tween20. The residual concentration of dimethyl sulfoxide was less than 0.1% in the binding assay and 0.8% in the competition assay.

Binding Assay. A solution of ET_ARs in VLiPs was incubated with TMR-ET-1 in VLiP binding buffer (50 mM Tris/HCl pH 7.4, 1 mM $CaCl_2$, 0.1% BSA, and 0.1% Tween20) at room temperature for 1−3 h. To measure nonspecific binding, an excess of 2 μM unlabeled ET-1 or, alternatively, reference ET_AR binding inhibitors (sarafotoxin 6b, BQ-123 and sulfisoxazole) in the same buffer was added to the control samples. To investigate the ET_AR in membrane fragments of CHO cells, the membranes were incubated with TMR-ET-1 in membrane binding buffer (50 mM Tris/HCl pH 7.4, 0.85 mM $CaCl_2$, 0.23% BSA, 1.6% glycerol, and 0.1% Tween20) at room temperature for 1−2 h. For stability measurements of VLiPs and membrane fragments, extended incubations times up to 24 h were applied. For the competition assay, the ligand TMR-ET-1 was premixed with an increasing concentration of competitor and then incubated with a solution of ET_ARs in VLiPs in the VLiP binding buffer at room temperature for 1−3 h.

For microscopic measurements, a sandwich was assembled from two microscope cover slips and two pieces of double sided, self-adhesive tape. The 200-μm thick tape was attached to the glass such that a 2-mm wide channel was formed in the middle, into which the sample solution was infused by capillary action. Alternatively, an AssayChip 24/25 with 24-wells from Evotec Technologies GmbH (Germany) was used. The sample volume was between 6 and 8 μL.

FCS/PCH Measurements and Data Analysis. The microscope was aligned and calibrated every day. The calibration procedure has been described earlier (*22*). The typical confocal volume dimensions of $\omega_r = 0.3$ μm and $\omega_z = 2.0$ μm were determined with Rhodamine 6G, a dye with a diffusion coefficient of 280 $\mu m^2/s$. Autocorrelation functions (ACFs) were recorded 10 times for 30 s, using a laser power of 35 μW. The 10 curves were averaged and fitted with a three-dimensional Gaussian model (*14*−*16*). Thereby, each data point was weighted with the standard deviation of the 10 measurements.

PCHs were recorded 10 times for 15 s, with a bin width of 50 μs (unless otherwise stated), while scanning the sample with a velocity of 0.8 μm/s on a circle with a radius of 30 μm. The 10 data sets were averaged and modeled with a theoretical curve based on the FIDA algorithm (*18*), using the generating function approach and a three-dimensional Gaussian observation volume. The free fluorophore was described by a single species (characterized by the concentration c_1 and its molecular brightness η_1), while the broad distribution of the number of fluorophores bound to the VLiPs was modeled by three species ($i = 2-4$), with their molecular brightness parameter being a multiple of the brightness of an individual fluorophore, $\eta_i = n_i \cdot \eta_1$. This four-species model was complemented by two contributions, one accounting for background depending on excitation light (e.g., scattered excitation light) and the other one independent of the excitation light (e.g., electronic noise). In the fitting procedure, the sum of the squared deviations between experimental data and model calculations was minimized to estimate the quality of the fits. The concentration of free ligand, c_L, was identified with the concentration of the first species, c_1, while the concentration of bound ligand, c_B, is given by the sum of the concentrations of species 2−4, weighted by their relative molecular brightness values, $n_i = \eta_i/\eta_1$

$$c_B = \sum_{4}^{i=2} c_i \cdot \frac{\eta_i}{\eta_1}$$

In the diagrams presented in this paper, the concentration data are averaged over three independent measurements, with the error bars representing the standard deviation.

RESULTS

Diffusion Coefficient and Absolute Concentration of TMR-ET-1. For the binding studies, we employed the ET-1 ligand that was fluorescently labeled with TMR on the lysine. Its absolute concentration was determined by FCS. In Figure 2, single species ACFs were fitted to the measured fluorescence intensity autocorrelation data. From the fit, a diffusion time of 227 ± 4 μs was determined (in this experiment, $\omega_r = 0.357$ μm), from which a diffusion coefficient of 140.5 ± 2.5 $\mu m^2/s$ was calculated. The determined diffusion coefficient corresponds to a spherical entity of about 3720 Da. Assuming a spherical shape of TMR-labeled ET-1 for simplicity, theory yields a diffusion coefficient of 153 $\mu m^2/s$ for the monomeric ligand. Comparison of the experimentally determined diffusion coefficient with the calculated one

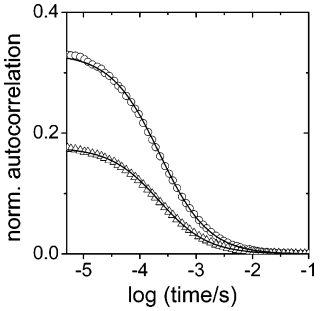

FIGURE 2: FCS determination of TMR-ET-1 concentration. The plot shows diffusion autocorrelation functions, with measured data (symbols) and best-fit model function (lines). From the fit parameters, concentrations of 3.298 ± 0.008 nM (○) and 6.177 ± 0.012 nM (△) were obtained. The diffusion times 229 ± 2 μs and 224 ± 2 μs correspond with $\omega_r = 0.357$ μm to diffusion coefficients of 139 ± 1 $\mu m^2/s$ and 142 ± 1 $\mu m^2/s$, respectively.

suggests that the TMR-ET-1 was largely monomeric in the concentration range of the binding studies presented below.

Additionally, the amplitude of the ACF depends on the average number of fluorescent molecules in the confocal observation volume and hence on the concentration. From the two ACFs shown in Figure 2, TMR-ET-1 concentrations of 3.3 nM and 6.2 nM were calculated, which agree with those expected from the dilution factor of the samples. For all other experiments, ligand concentrations were determined from FCS data.

Even with excitation laser powers 10-fold larger than those used in the FCS and FIDA experiments reported here (data not shown), we observed a linear power dependence of the TMR-ET-1 fluorescence emission. Consequently, photobleaching of TMR-ET-1 was negligible in these experiments.

FIDA Measurements of TMR-ET-1 to ET_AR Binding in a Scanning Approach. Instead of analyzing the temporal fluctuations of the fluorescence signal as is done in FCS, one can also analyze the statistics of the intensities of the generated photon bursts. The distribution of the number of photons per time bin can be analyzed by a statistical method referred to as FIDA (see Experimental Procedures). FIDA allows us to distinguish differently bright species (free TMR-ET-1 and VLiPs with various numbers of receptors occupied by TMR-ET-1) in the sample mixture and to determine their individual concentrations. As VLiPs are large and diffuse rather slowly (diffusion coefficient ~3 ± 2 $\mu m^2/s$), a long data acquisition time is needed to generate enough events of VLiPs passing randomly through the confocal volume. This can be partially compensated by a scanning approach, based on an active search for vesicles in the sample by moving the focused laser beam or the entire sample, so that many more vesicles with bound ligands can be detected during the same data collection time (Figure 3). To optimize the scan velocity, the sample (10 nM ET_AR in VLiPs incubated with 2 nM TMR-ET-1) was measured with or without scanning, using different scan velocities for the same total data acquisition time (3 times, 10 s). Using a bin width of 100 μs, the largest number of events with large photon numbers was detected at a scan velocity of 0.8 μm/ms (Figure 3). Similar results were obtained for bin widths of 10 and 50 μs (data not shown). Therefore, we decided to use a scan velocity of 0.8 μm/ms in all the following experiments. The scanning technique allowed us to significantly reduce the data acquisition time without loss of data quality.

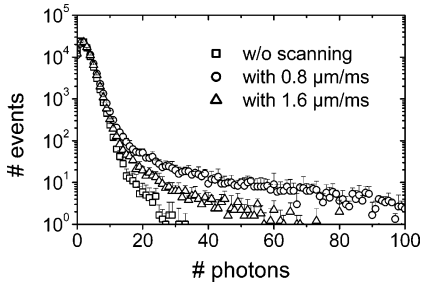

FIGURE 3: PCHs with and without scanning in the sample. A solution of 10 nM ET_A receptors in VLiPs was incubated with 2 nM TMR-ET-1. The sample was measured without (□) or with scanning at scan velocities of 0.8 μm/ms (○) and 1.6 μm/ms (△) for the same time (3 × 10 s). The width of the time bins used here was 100 μs.

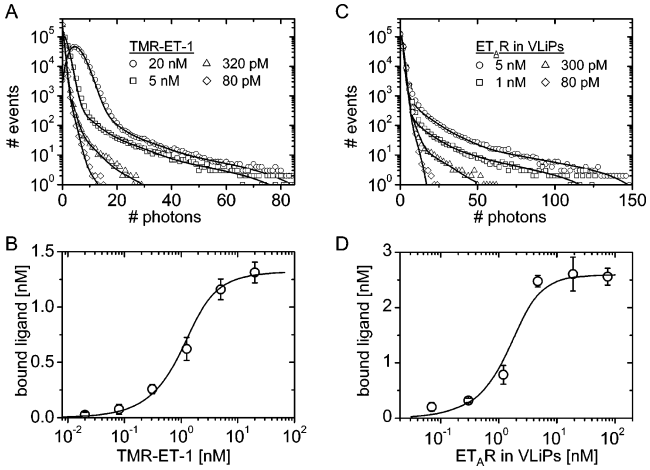

FIGURE 4: TMR-ET-1 binding to its receptor in VLiPs. (A) Photon counting histograms (symbols) of a ligand titration experiment. A solution of 1.5 nM ET_ARs in VLiPs was incubated with the concentrations of TMR-ET-1 given in the figure. The solid lines describe the PCHs by a four-species model. (B) The binding curve of the ligand titration experiment resulting from the PCH analysis. The fit (solid line) yields $K_D = 0.5 \pm 0.2$ nM. (C) Photon counting histograms (symbols) of a receptor titration experiment. A solution of 2 nM TMR-ET-1 was incubated with indicated concentrations of ET_ARs in VLiPs. The data were modeled by a four species model (solid lines). (D) Binding curve derived from the data in panel C. The fit (solid line) yields $K_D = 0.3 \pm 0.2$ nM.

K_D Determination for the Binding of TMR-ET-1 to VLiP-Integrated ET_AR. The fluorescence of TMR-ET-1 upon binding to the receptor does not change, as was checked in prior experiments on bulk samples. In a ligand titration experiment, 1.5 nM VLiP-integrated ET_ARs were incubated with different concentrations of TMR-ET-1 in the range from 20 pM to 20 nM. To investigate the nonspecific binding, an excess of unlabeled ligand ET-1 was added to control samples, which were identically incubated and measured. A selection of the recorded PCHs is shown in Figure 4A. With increasing concentrations of TMR-ET-1, the number of events with high photon number increased. This observation indicates a higher occupancy of ET_ARs with fluorescent ligands and thus increased brightness of the VLiPs.

FIDA/PCH analysis was carried out with a four-species model, using the algorithms described in Experimental Procedures. One species represents the free ligand, and the other three species represent the brighter VLiP particles with different numbers of bound ligands. The restriction to three brightness values for the differently ligand-occupied VLiPs

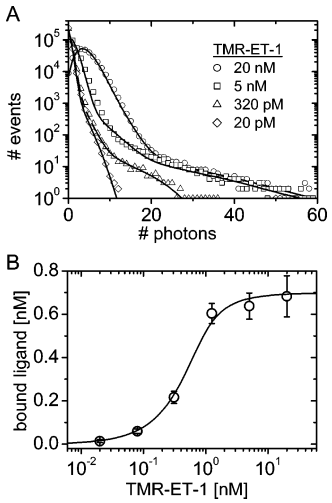

FIGURE 5: TMR-ET-1 binding to its receptor in membrane fragments. (A) Photon counting histograms (symbols) of a ligand titration experiment. A solution of ET_ARs in membrane fragments was incubated with various concentrations of TMR-ET-1, as listed in the figure. The solid lines describe the PCHs by a four-species model. (B) The resulting binding curve of the ligand titration experiment. The fit (solid line) yields $K_D = 0.2 \pm 0.1$ nM.

is arbitrary. Our experimental results, however, indicate that this model describes the brightness distribution sufficiently well with respect to the binding experiments. The concentration of bound ligand was calculated from the FIDA-determined concentrations of the three assumed VLiP-ligand species multiplied by their individual FIDA-determined brightness values. Thus, the analysis yielded the concentration of free as well as bound TMR-ET-1, and their sum was in agreement with the total concentration of TMR-ET-1 used in the experiment (as determined by FCS). The sum of the fluorescence intensities of the species, weighted by their particle numbers, and the background contributions was also in agreement with the overall photon count rate. The analysis of the recorded PCHs of control samples with an excess of unlabeled ET-1 showed that nonspecific binding was negligible (data not shown). Nevertheless, nonspecific binding was subtracted from the binding data.

The resulting concentrations of bound ligand are plotted in Figure 4B versus the total ligand concentration. The fitted binding curve of the ligand titration experiment yields a K_D value of 0.5 ± 0.2 nM. From the molecular brightness of ligand-saturated VLiPs, a maximum number of ET_ARs per VLiP of about 100 was estimated.

In a second experiment, the roles of receptor and ligand were exchanged, and a solution of 2 nM TMR-ET-1 was titrated with VLiP-integrated ET_ARs at concentrations ranging from 80 pM to 75 nM. As the recorded PCHs show, the number of events with high photon number grew with increasing concentration of VLiPs (Figure 4C) due to the increasing number of bound fluorescent ligands.

In Figure 4D, the FIDA-determined concentrations of bound ligand are plotted versus the concentration of ET_ARs integrated in VLiPs. A K_D value of 0.3 ± 0.2 nM was obtained from fitting a binding curve to the receptor titration data.

K_D Determination for the Binding of TMR-ET-1 to ET_AR Embedded in Membrane Fragments. Plasma membrane fragments isolated from mammalian cells overexpressing the

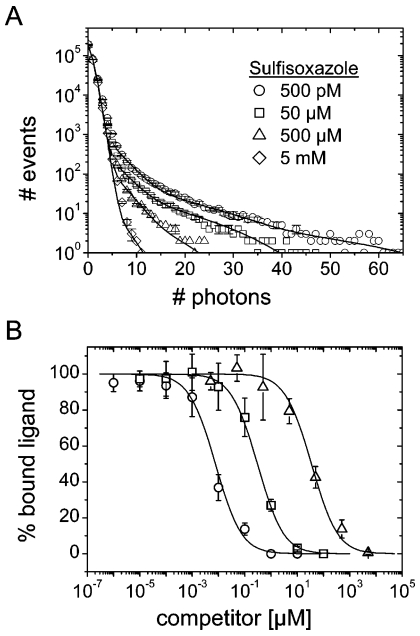

FIGURE 6: Binding competition by sarafotoxin 6b, BQ-123 and sulfisoxazole. A solution of 1.5 nM ET_ARs in VLiPs was incubated with 2 nM TMR-ET-1 and with indicated concentrations of competitor. (A) Photon counting histograms (symbols) of a competition experiment with sulfisoxazole. The data were also analyzed with a four-species model (lines). (B) Results of competition experiments with sarafotoxin 6b (○), or BQ-123 (□) or sulfisoxazole (△) shown as a ratio of bound ligand with and without competitor versus competitor concentration. As the nonspecific binding was negligible, we neglected it in the experimental evaluation. The fits (solid lines) yielded $K_i = 0.8 \pm 0.2$ nM for sarafotoxin 6b, 32 ± 5 nM for BQ-123 and 3.6 ± 0.8 μM for sulfisoxazole.

receptor of interest have proven to be successful tools to integrate transmembrane proteins with a physiological receptor−ligand binding profile. Therefore, we compared the properties of ET_AR-chimeric VLiPs with membrane fragments from ET_AR-overexpressing CHO cells using the same FIDA technique.

For this purpose, a solution of ET_ARs in membrane fragments was titrated with TMR-ET-1 in the concentration range from 20 pM to 20 nM. A selection of the recorded PCHs is shown in Figure 5A. With increasing concentration of membrane fragment-embedded ET_A-receptors, the number of events with high photon number increased. This correlates with an increased number of bound fluorescent ligands per membrane fragment. From the maximum count rate, we could estimate that the purchased single-membrane fragments contained up to 100 ET_ARs. The measured PCH data (Figure 5A) were modeled by the four-species model that was already applied to the VLiP data analysis. The resulting concentrations of bound ligand are plotted in Figure 5B versus the total ligand concentration. The fit of the ligand titration data with a binding curve yielded $K_D = 0.2 \pm 0.1$ nM.

Ligand Competition Experiments with Reference Compounds. The binding properties of the VLiP-integrated ET_AR were further analyzed in ligand competition experiments, using ligand-competitive binders of the ET_AR with agonistic (sarafotoxin S6b) or antagonistic properties (sulfisoxazole and BQ-123). A solution of 1.5 nM ET_AR in VLiPs was incubated with 2 nM TMR-ET-1 and with varying concentrations of competitor compounds. Figure 6A shows a

selection of PCHs for the competitor compound sulfisoxazole. The events with high photon number decreased with increasing concentration of the competitor, showing the displacement of the bound fluorescent ligand by the nonfluorescent competitor.

The PCH data of the three competitors were analyzed as described above. In all experiments, we observed the displacement of the TMR-ET-1 ligand by the competitor compound, as shown in Figure 6B, where the percentage of bound ligand is plotted against the competitor concentration. The fits of the competition curves yielded K_i values of 0.8 $\pm$ 0.2 nM, 32 $\pm$ 5 nM, and 3.6 $\pm$ 0.8 μM for sarafotoxin 6b, BQ-123, and sulfisoxazole, respectively.

DISCUSSION

All methods applied in high-throughput screening (HTS) of membrane proteins, including assays based on confocal detection techniques such as FIDA, require membrane fractions (vesicles, fragments) in which the protein of interest is present at a high concentration and in its normal physiological function. VLiPs that express the transmembrane protein of interest may fulfill these requirements. To validate the applicability of VLiPs to the drug discovery process, we investigated their properties in binding experiments and their suitability for fluorescence fluctuation spectroscopy assays.

In preparation to our ligand−receptor binding experiments, we first measured the diffusion coefficient of TMR-ET-1 in an FCS experiment. Fluorophores, and consequently, fluorophore-labeled biomolecules, often tend to aggregate in aqueous solutions because of the hydrophobic nature of the fluorophores. However, a diffusion ACF curve for a single species gave a good fit to the experimental data, and the resulting diffusion coefficient corresponded to a monomeric state of the TMR-ET-1. Note that a minor portion of the dimeric ligand against mostly monomeric ligand is not detectable by the FCS method. Another advantageous feature of the FCS analysis is the possibility to perform a precise measurement of the concentration of a fluorophore-labeled species. This form of concentration determination is superior to methods that rely on weighed quantities and do not account for losses due to, for example, nonspecific binding of the fluorophore-labeled entity to the surfaces of the sample cell. We thus used FCS to determine the absolute concentration of the TMR-ET-1 in solution for our titration experiments.

A problem associated with fluorescence fluctuation experiments on particles that diffuse slowly is the long data acquisition time needed to generate enough statistical events for FIDA or FCS. With a diffusion coefficient of $\sim$3 $\mu m^2/s$, the VLiPs fall into this category of slowly diffusing entities. Therefore, we employed a scanning approach, which is based on an active search for VLiPs or membrane fragments in the sample by moving the focused laser beam or the entire sample. Our FIDA data clearly showed that many more VLiPs with bound ligands can be detected within the same data collection time by scanning. For FIDA, the scan velocity needs to be optimized for a large number of VLiPs detected during the measurement time, while ensuring a reasonably long residence time of the detected VLiP in the moving confocal volume, so that sufficiently large photon numbers appear within the time bin chosen. In our experiments, a scan velocity of 0.8 μm/ms produced the largest number of events with high photon counts. The measurement time is an important issue, particularly for HTS applications. For these cases, the scanning technique allows a substantial reduction of the measurement time without loss of data quality.

In principle, FCS may also be used for binding measurements because it can distinguish between small free ligands and large VLiPs with bound ligands (*23*, *24*) on the basis of their different diffusion times through the confocal observation volume. However, the long data acquisition time needed to generate enough statistical events in FCS analysis cannot be as efficiently shortened as in FIDA by using the above-described scanning approach (data not shown, (*25*)).

Active recruitment of the ET_ARs to the budding VLiP is mediated by the interaction between the ET_AR-tag and the Gag-tag. Therefore, the concentration of ET_ARs in the VliP lipid bilayer is rather high, and one has to ensure that the close proximity of the receptors does not cause an energy transfer between the fluorescently labeled ligands. Based on the observation that the average fluorescence intensity of the sample did not change upon receptor-saturating ligand binding, we can exclude such a self-quenching process.

To determine K_D values for the interaction between VLiP-incorporated ET_ARs and TMR-ET-1, we performed FIDA experiments at different ligand and receptor concentrations. A titration of TMR-ET-1 against a constant VLiP-ET_AR concentration and a titration of VLiP-ET_AR against a constant TMR-ET-1 concentration resulted in similar K_D values of 0.5 and 0.3 nM, respectively. To saturate the ET_ARs with TMR-ET-1 in the ligand titration experiments, TMR-ET-1 concentrations up to 20 nM were used. At these high ligand concentrations, however, several unbound ligands are present in the confocal observation volume on average. Under these conditions, FIDA analysis faces the problem that one cannot distinguish between free and bound ligands. Therefore, instead of titrating a fixed receptor concentration with varying ligand concentrations, titrating the receptor against a fixed concentration of the fluorophore-labeled ligand in the lower nanomolar range is more suitable for a K_D determination using FIDA. To reach ligand saturation in this receptor titration approach, high concentrations of receptor were required. Here, another advantageous feature of the ET_AR-enriched VLiPs became apparent: a VLiP stock suspension with $\sim$150 nM ET_AR was available. In contrast, only $\sim$4 nM ET_AR stock suspensions were available for the membrane fragments. Therefore, the K_D determination for the membrane fragment-embedded ET_ARs could only be carried out in the ligand titration mode, with a fixed, lower nanomolar concentration of ET_AR. The membrane fragments were derived from CHO cells overexpressing the ET_AR. It is well accepted that plasma membrane fragments isolated from mammalian cells overexpressing the receptor of interest display receptor proteins with a normal receptor−ligand binding profile. The FIDA-determined K_D values of 0.3−0.5 nM for the ET_ARs integrated into VLiPs are close to the K_D value of 0.2 nM for the ET_ARs in their physiological biomembrane environment. The CHO membrane fragments that we used for our binding experiments contained a rather high ET_AR density (2.4 pmol/mg membrane protein). Cell lines that overexpress the receptor of interest to a similar extent are not available for all GPCRs. Thus, the use of receptor-enriched VliPs will be particularly advantageous for

applications in which the receptor density in membrane fragments from receptor-overexpressing cells is low. Furthermore, we found that VLiPs were stable for about 24 h in some long-time incubation binding experiments. In contrast, membrane fragments were stable for only 2−3 h under the same assay conditions (data not shown). The better stability is a further advantage of VLiPs that makes them interesting tools in the drug discovery process.

The FIDA-determined K_D values for the VLiP-integrated ET_AR are close to the K_D of 0.64 nM and 0.22 nM, obtained with [125I]-ET-1 in radioligand assays using human ET_AR in homogenates of human saphenous vein (*26*) and ET_AR overexpressed in baby hamster kidney (BHK) cells (*27*), respectively. This comparison with literature data on tissue or cell surface-expressed receptors supports the normal binding profile of the VLiP-integrated ET_ARs. However, K_D values in the range between 0.01 and 5 nM for binding of ET-1 to ET_AR were reported in a review article (*28*). Such a large range of the dissociation constants can have numerous reasons. First, different tissues and cell types were investigated. In tissues or cells, other cooperating or inhibiting proteins can be involved in the binding of ET-1 to its receptor. For example, interactions between ET_AR and endothelin B receptor were discussed for the rat anterior pituitary gland (*29*, *30*). Second, the methods used to measure the K_D values are very different. The most frequently used technique is the radioligand binding assay, which necessitates separation steps to wash out the unbound radioligand. Apart from the radioligand binding assay format, there are technically more complicated experimental procedures, for example, the measurement of the dependence of guinea pig bronchial contraction on ET-1 (*31*). These assay formats do not assess ligand binding directly but rather measure secondary effects that may be nonlinear with respect to the receptor occupancy. In this context, a discrepancy between contraction measurements and a radioligand binding assay was observed for ET_AR in sheep isolated tracheal smooth muscle (*32*). While such measurements constitute important functional studies, radioligand binding assays or FIDA measurements are more appropriate for a biochemical determination of a K_D value.

In comparison to radioligand binding assays, there are some important advantages of the FIDA technique. First, no separation of bound from unbound ligand is required for the homogeneous FIDA assay format, which is time-saving and thus of particular importance for HTS applications. Second, we can determine the concentrations of both free and bound ligand in one measurement. This is a useful control in every FIDA measurement, whereas only the amount of bound ligand is measured in a radioligand binding assay. Third, in FIDA, the fluorescence is detected in a confocal observation volume of about 1 femtoliter, independent of the total assay volume. Therefore, the FIDA signal is insensitive to miniaturization, as has already been demonstrated (*20*). Particularly in HTS, low assay volumes save the biological material as well as the precious compounds, which are tested for their potential bioactivity.

For sarafotoxin 6b, our K_i value of 0.8 nM is close to those reported in the literature (0.55 nM (*26*); 0.6 nM (*33*)). Likewise, the K_i value of 32 nM for BQ-123 determined in this work corresponds well to previously reported values (19 nM (*34*), 40 nM (*35*), 21.3 nM (*36*)). However, K_i values in the lower nanomolar range for BQ-123 have also been reported. For example, Desmarets and Frelin (*37*) determined a K_i of 2 nM for BQ-123. However, in their study, a comparatively low K_D of 5−7 pM for ET-1 was measured, suggesting that a technical problem may have caused these deviations. Our K_i of 3.6 μM for sulfisoxazole is 3-fold higher than the K_D obtained from the inhibition of ET-1 stimulated phosphoinositide hydrolysis measured in TE 671 cells (*38*). Consequently, all K_i values determined by our FIDA experiments were similar to literature values that were obtained for the respective compounds with membrane fragments, intact cells or tissues. In summary, our results indicate that the ET_ARs integrated into the outer lipid bilayer of VLiPs maintain their physiological properties with regard to the TMR-ET-1 ligand and with regard to a series of pharmacologically active compounds.

In the search for novel GPCR-directed drugs, assay formats are required that can be miniaturized that do not rely on separation steps (e.g., free ligand from bound ligand), and that still maintain the receptor of interest in a possibly physiological environment. The use of VLiP-integrated GPCRs in combination with FIDA has great potential to benefit the drug discovery process in the pharmaceutical industry. We expect a substantially increased use of this novel confocal technique for highly miniaturized biochemical assays soon.

ACKNOWLEDGMENT

We thank Martin J. Valler, Elza Amirgoulova, Don C. Lamb, Carlheinz Röcker, and Vladimir Ens for assistance throughout the project. We are greatly indebted to Birgit Hecks, Kathrin Adlkofer, Leif Brand, Rudolf Zirwes, and Martin Pitschke for technical advice and helpful discussions.

REFERENCES

1. Drews, J. (2000) Drug discovery: a historical perspective, *Science 287*, 1960−1964.
2. Ma, P., and Zemmel, R. (2002) Value of novelty?, *Nat. Rev. Drug Discov. 1*, 571−572.
3. Gheysen, D., Jacobs, E., de Foresta, F., Thiriart, C., Francotte, M., Thines, D., and De Wilde, M. (1989) Assembly and release of HIV-1 precursor Pr55gag virus-like particles from recombinant baculovirus-infected insect cells, *Cell 59*, 103−112.
4. Hughes, B. P., Booth, T. F., Belyaev, A. S., McIlroy, D., Jowett, J., and Roy, P. (1993) Morphogenic capabilities of human immunodeficiency virus type 1 gag and gag-pol proteins in insect cells, *Virology 193*, 242−255.
5. Morikawa, S., Booth, T. F., and Bishop, D. H. (1991) Analyses of the requirements for the synthesis of virus-like particles by feline immunodeficiency virus gag using baculovirus vectors, *Virology 183*, 288−297.
6. Royer, M., Cerutti, M., Gay, B., Hong, S. S., Devauchelle, G., and Boulanger, P. (1991) Functional domains of HIV-1 gag-polyprotein expressed in baculovirus-infected cells, *Virology 184*, 417−422.
7. Zhou, W., Parent, L. J., Wills, J. W., and Resh, M. D. (1994) Identification of a membrane-binding domain within the amino-terminal region of human immunodeficiency virus type 1 Gag protein which interacts with acidic phospholipids, *J. Virol. 68*, 2556−2569.
8. Yamshchikov, G. V., Ritter, G. D., Vey, M., and Compans, R. W. (1995) Assembly of SIV virus-like particles containing envelope proteins using a baculovirus expression system, *Virology 214*, 50−58.
9. Delchambre, M., Gheysen, D., Thines, D., Thiriart, C., Jacobs, E., Verdin, E., Horth, M., Burny, A., and Bex, F. (1989) The GAG precursor of simian immunodeficiency virus assembles into virus-like particles, *EMBO J. 8*, 2653−2660.

10. Luo, L., Li, Y., and Kang, C. Y. (1990) Expression of gag precursor protein and secretion of virus-like gag particles of HIV-2 from recombinant baculovirus-infected insect cells, *Virology 179*, 874−880.
11. Bremnes, T., Paasche, J. D., Mehlum, A., Sandberg, C., Bremnes, B., and Attramadal, H. (2000) Regulation and intracellular trafficking pathways of the endothelin receptors, *J. Biol. Chem. 275*, 17596−17604.
12. Yanagisawa, M., Kurihara, H., Kimura, S., Tomobe, Y., Kobayashi, M., Mitsui, Y., Yazaki, Y., Goto, K., and Masaki, T. (1988) A novel potent vasoconstrictor peptide produced by vascular endothelial cells, *Nature 332*, 411−415.
13. Hosoda, K., Nakao, K., Tamura, N., Arai, H., Ogawa, Y., Suga, S., Nakanishi, S., and Imura, H. (1992) Organization, structure, chromosomal assignment, and expression of the gene encoding the human endothelin-A receptor, *J. Biol. Chem. 267*, 18797−18804.
14. Aragon, S. R., and Pecora, R. (1975) Fluorescence correlation spectroscopy and Brownian rotational diffusion, *Biopolymers 14*, 119−137.
15. Elson, E. L., and Madge D. (1974) Fluorescence Correlation Spectroscopy, I: Conceptual Basis and Theory, *Biopolymers 13*, 1−27.
16. Lamb, D. C., Schenk, A., Rocker, C., Scalfi-Happ, C., and Nienhaus, G. U. (2000) Sensitivity enhancement in fluorescence correlation spectroscopy of multiple species using time-gated detection, *Biophys. J. 79*, 1129−1138.
17. Chen, Y., Muller, J. D., So, P. T., and Gratton, E. (1999) The photon counting histogram in fluorescence fluctuation spectroscopy, *Biophys. J. 77*, 553−567.
18. Kask, P., Palo, K., Ullmann, D., and Gall, K. (1999) Fluorescence-intensity distribution analysis and its application in biomolecular detection technology, *Proc. Natl. Acad. Sci. U. S. A 96*, 13756−13761.
19. Klumpp, M., Scheel, A., Lopez-Calle, E., Busch, M., Murray, K. J., and Pope, A. J. (2001) Ligand binding to transmembrane receptors on intact cells or membrane vesicles measured in a homogeneous 1-microliter assay format, *J. Biomol. Screen. 6*, 159−170.
20. Rudiger, M., Haupts, U., Moore, K. J., and Pope, A. J. (2001) Single-molecule detection technologies in miniaturized high throughput screening: binding assays for g protein-coupled receptors using fluorescence intensity distribution analysis and fluorescence anisotropy, *J. Biomol. Screen. 6*, 29−37.
21. Scheel, A. A., Funsch, B., Busch, M., Gradl, G., Pschorr, J., and Lohse, M. J. (2001) Receptor−ligand interactions studied with homogeneous fluorescence-based assays suitable for miniaturized screening, *J. Biomol. Screen. 6*, 11−18.
22. Schenk, A., Ivanchenko, S., Rocker, C., Wiedenmann, J., and Nienhaus, G. U. (2004) Photodynamics of red fluorescent proteins studied by fluorescence correlation spectroscopy, *Biophys. J. 86*, 384−394.
23. Auer, M., Moore, K. J., Meyer-Almes, F. J., Guenther, R., Pope, A. J., and Stoeckli, K. (1998) Fluorescence correlation spectroscopy: lead discovery by miniaturized HTS, *Drug Discov. Today 3*, 457−465.
24. Zemanova, L., Schenk, A., Valler, M. J., Nienhaus, G. U., and Heilker, R. (2003) Confocal optics microscopy for biochemical and cellular high-throughput screening, *Drug Discov. Today 8*, 1085−1093.
25. Eggeling, C., Brand, L., Ullmann, D., and Jager, S. (2003) Highly sensitive fluorescence detection technology currently available for HTS, *Drug Discov. Today 8*, 632−641.
26. Maguire, J. J., Kuc, R. E., Rous, B. A., and Davenport, A. P. (1996) Failure of BQ123, a more potent antagonist of sarafotoxin 6b than of endothelin-1, to distinguish between these agonists in binding experiments, *Br. J. Pharmacol. 118*, 335−342.
27. Hechler, U., Becker, A., Haendler, B., and Schleuning, W. D. (1993) Stable expression of human endothelin receptors ETA and ETB by transfected baby hamster kidney cells, *Biochem. Biophys. Res. Commun. 194*, 1305−1310.
28. Davenport, A. P. (1997) Distribution of endothelin receptors, in *Endothelin in Biology and Medicine* (Mille, R., Pelton, J. T., and Huggins, J., Eds.) pp 45−68, CRC Press, Boca Raton, FL.
29. Himeno, A., Shigematsu, K., Taguchi, T., and Niwa, M. (1998) Endothelin-1 binding to endothelin receptors in the rat anterior pituitary gland: interaction in the recognition of endothelin-1 between ETA and ETB receptors, *Cell Mol. Neurobiol. 18*, 447−452.
30. Harada, N., Himeno, A., Shigematsu, K., Sumikawa, K., and Niwa, M. (2002) Endothelin-1 binding to endothelin receptors in the rat anterior pituitary gland: possible formation of an ETA-ETB receptor heterodimer, *Cell Mol. Neurobiol. 22*, 207−226.
31. Hay, D. W., and Luttmann, M. A. (1997) Nonpeptide endothelin receptor antagonists. IX. Characterization of endothelin receptors in guinea pig bronchus with SB 209670 and other endothelin receptor antagonists, *J. Pharmacol. Exp. Ther. 280*, 959−965.
32. Henry, P. J., and King, S. H. (1999) Typical endothelin ETA receptors mediate atypical endothelin-1-induced contractions in sheep-isolated tracheal smooth muscle, *J. Pharmacol. Exp. Ther. 289*, 1385−1390.
33. Cain, M. J., Garlick, R. K., and Sweetman, P. M. (1991) Endothelin-1 receptor binding assay for high throughput chemical screening *J. Cardiovasc. Pharmacol. 17 Suppl 7*, S150−S151.
34. Raschack, M., Unger, L., Riechers, H., and Klinge, D. (1995) Receptor selectivity of endothelin antagonists and prevention of vasoconstriction and endothelin-induced sudden death, *J. Cardiovasc. Pharmacol. 26 Suppl 3*, S397−S399.
35. Nambi, P., Pullen, M., Wu, H. L., Lee, D., Saunders, D., Heys, R., Aiyar, N., Leber, J., Elliott, J., Brooks, D., Ohlstein, E., and Ruffolo, R. (1996) Nonpeptide endothelin receptor antagonists. VII: Binding characteristics of [3H]SB 209670, a novel nonpeptide antagonist of endothelin receptors, *J. Pharmacol. Exp. Ther. 277*, 1567−1571.
36. Servitja, J. M., Masgrau, R., Sarri, E., and Picatoste, F. (1998) Involvement of ET(A) and ET(B) receptors in the activation of phospholipase D by endothelins in cultured rat cortical astrocytes, *Br. J. Pharmacol. 124*, 1728−1734.
37. Desmarets, J., and Frelin, C. (1999) High affinity interaction of endothelin-3 with recombinant ETA receptors, *Biochem. Biophys. Res. Commun. 256*, 357−360.
38. Chan, M. F., Okun, I., Stavros, F. L., Hwang, E., Wolff, M. E., and Balaji, V. N. (1994) Identification of a new class of ETA selective endothelin antagonists by pharmacophore directed screening, *Biochem. Biophys. Res. Commun. 201*, 228−234.

BI035901+